

Multiwalled carbon nanotubes for stray light suppression in space flight instruments

John G. Hagopian, Stephanie A. Getty, Manuel Quijada, June Tveekrem, Ron Shiri, Patrick Roman, James Butler, Georgi Georgiev, Jeff Livas, Cleophus Hunt, Alejandro Maldonado
NASA Goddard Space Flight Center (United States);

Saikat Talapatra, Xianfeng Zhang,
Southern Illinois University (United States);

Stergios J. Papadakis, Andrew H. Monica, David Deglau
Johns Hopkins University Applied Physics Laboratory (United States)

ABSTRACT

1. INTRODUCTION

Observations of the Earth are extremely challenging; its large angular extent floods scientific instruments with high flux within and adjacent to the desired field of view. This bright light diffracts from instrument structures, rattles around and invariably contaminates measurements. Astrophysical observations also are impacted by stray light that obscures very dim objects and degrades signal to noise in spectroscopic measurements. Stray light is controlled by utilizing low reflectance structural surface treatments and by using baffles and stops to limit this background noise. In 2007 GSFC researchers discovered that Multiwalled Carbon Nanotubes (MWCNTs) are exceptionally good absorbers, with potential to provide order-of-magnitude improvement over current surface treatments and a resulting factor of 10,000 reduction in stray light when applied to an entire optical train. Development of this technology will provide numerous benefits including: a.) simplification of instrument stray light controls to achieve equivalent performance, b.) increasing observational efficiencies by recovering currently unusable scenes in high contrast regions, and c.) enabling low-noise observations that are beyond current capabilities. Our objective was to develop and apply MWCNTs to instrument components to realize these benefits. We have addressed the technical challenges to advance the technology by tuning the MWCNT geometry using a variety of methods to provide a factor of 10 improvement over current surface treatments used in space flight hardware. Techniques are being developed to apply the optimized geometry to typical instrument components such as spiders, baffles and tubes. Application of the nanostructures to alternate materials (or by contact transfer) is also being investigated. In addition, candidate geometries have been tested and optimized for robustness to survive integration, testing, launch and operations associated with space flight hardware. The benefits of this technology extend to space science where observations of extremely dim objects require suppression of stray light.

1.1 Motivation for improved stray light control

The National Research Council's (NRC) decadal survey document titled, "Earth Science and Applications from Space: National Imperatives for the Next Decade and Beyond [1]," outlines a multi-mission, multi-instrument science and engineering remote sensing program to understand our changing planet with the goals of maximizing economic competitiveness and societal benefits." Climate change [2] and variability are specifically called out in the decadal survey as having significant societal impacts over the course of the next two decades. With respect to climate change and variability, the decadal survey specifically states that "the link between climate research and societal benefit will require a much greater emphasis on higher spatial resolution in climate predictions, observations, and assessments." In addition, the decadal survey recommends that United States civilian space agencies, of which NASA and NOAA are leads, aggressively pursue new technology needed to support necessary missions.

The radiometric and imaging properties of any remote sensing instrument are tied to its within, near, and far field point spread function and stray light performance [3]. The optical design, characterization, and performance of Earth remote sensing instruments in these areas have proven to be challenging. Near and far-field optical performance depends on the

diffraction and stray light suppression characteristics of an instrument and involves characterizing the multi-wavelength bidirectional scatter properties of an instrument's mirrors, apertures, baffles, vanes, and scan cavities. Initial studies on the near field and far field reflectance of MultiWalled Carbon NanoTubes (MWCNTs) show promise of a significant improvement over commonly used paints and surface treatments in stray light control and a reduction in diffraction over large operating optical wavelength and dynamic ranges. The benefits to remote sensing science of the improved spatial and radiometric performance realized through the application of MWCNT technology is best illustrated by briefly examining the potential improvements to the most challenging Earth Science measurements, namely ocean color/chlorophyll and cloud/aerosol interaction.

1.2 Ocean Color/Chlorophyll Example

Probably the most radiometrically challenging and climate sensitive Earth science measurement is satellite remote sensing of ocean color/chlorophyll. The ocean is an optically dark target in the visible and near infrared and often dotted with numerous bright clouds. It is globally sensed by the SeaWiFS and MODIS instruments approximately every 2 days. However, approximately 1 week is required to obtain a complete global ocean sampling from these instruments due to clouds. As shown in Figure 1, improvements in near and far-field stray light performance realized through the use of MWCNTs on instrument optical and stray light surfaces would increase the number of chlorophyll retrievable pixels by 32%. This constitutes a significant improvement in global coverage for the study of ocean color/chlorophyll. Improved spatial and radiometric performance realized by the application of MWCNT technology will also improve the ability to perform science in coastal zones and in captured bodies of water, such as the Chesapeake Bay.

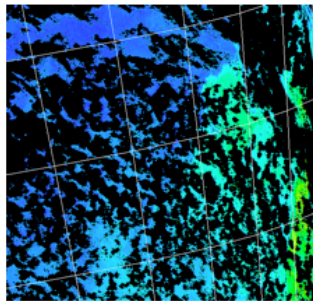
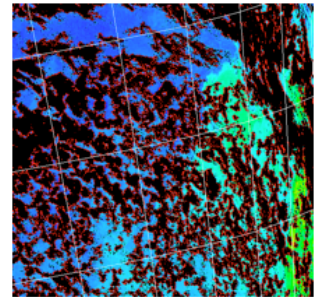


Figure 1. Chlorophyll concentration derived from SeaWiFS images of the S. Pacific off the coast of Chile. Chlorophyll concentrations decrease from yellow to blue, and black represents areas where chlorophyll is not retrievable (e.g. clouds). On the left is a chlorophyll concentration image in which chlorophyll is not derived around clouds due to stray light contamination (i.e. those areas are set to black). The right shows in red the extent of the regions in the left image, which were contaminated with stray light. The reduction in stray light levels afforded by MWCNT technology would enable chlorophyll to be confidently retrieved in all red areas, leading to a 32% increase in scientifically useful pixels.



2. CHARACTERIZATION OF OPTICAL PROPERTIES

For specular reflectance, the angle of reflection is equal to the angle of incidence on the substrate; direct reflection off of structural elements is carefully controlled. In most optical instruments the source of stray light that is more difficult to control is that scattered at all angles. This light can be reflected many times and find its way to the instrument focal plane where it can degrade the observations by creating noise that obscures the signal of interest. Initial specular reflectance measurements of oriented MWCNTs fabricated at GSFC had much lower reflectance than randomly oriented carbon nanotube samples. The difference however, is much smaller when all the light that is reflected from the samples is measured as shown in Figure 2. Therefore it is critical that the correct means of characterizing any candidate stray light controls be utilized to evaluate the various fabricated samples.

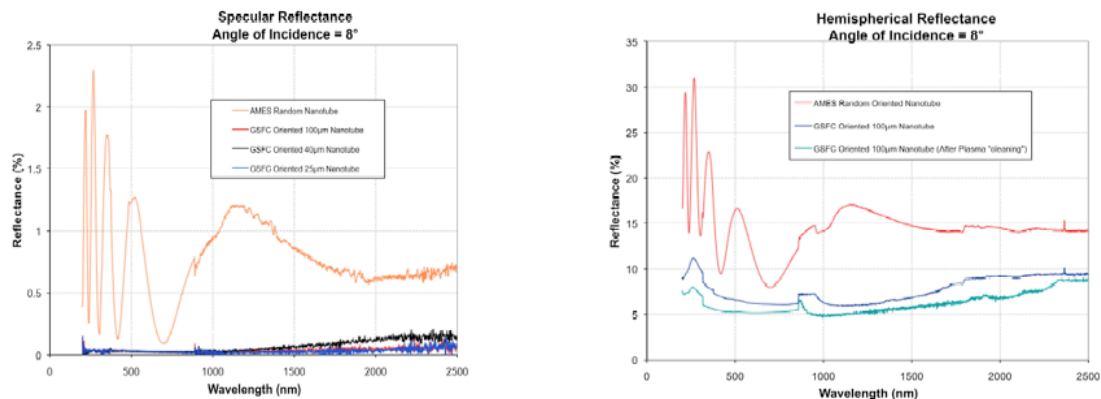


Figure 2. Comparison of specular and hemispherical reflectance

2.1 Hemispherical Reflectance

Hemispherical reflectance is a measure of all light that is scattered off of a test sample, this is also known as total integrated scatter or TIS. The instrument used to measure the hemispherical reflectance is a double monochromator PE950 grating instrument equipped with an integrating sphere accessory as shown in Figure 3. Beam paths within the accessory are illustrated in this figure as well. Light entering the accessory is directed to one of two entrance ports on the sphere: the reference beam and sample beams. The reference beam enters the integrating sphere via a rectangular opening adjacent to M5. The sample beam is reflected into the sphere directly off mirror M2 and onto the sample to be measured. This configuration allows the capture of all the reflected light from the sample. This light detection is done by two detectors located inside the sphere: A lead sulfide (PbS) detector to cover the 860-2500 nm and a R955 photomultiplier tube (PMT) for the wavelength range between 200 and 860 nm. Finally the inside of the sphere is coated with a spectralon coating. The measurement of hemispherical reflectance does not discriminate the angle of reflectance only the total amount of light. Hemispherical reflectance is a good measure of the relative ability of materials to absorb light and therefore a good screening tool to determine if a particular recipe is effective, it does not however provide the full range of characterization required for modeling an instrument to determine system stray light.

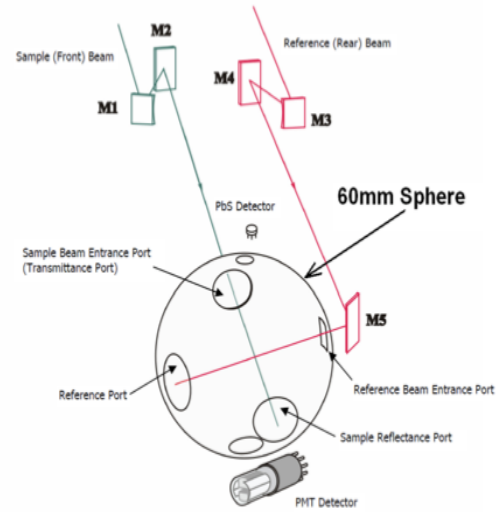


Figure 3. Hemispherical reflectance configuration

2.2 Bidirectional Reflectance Distribution Function (BRDF)

While hemispherical reflectance or total integrated scatter quantifies the total amount of light that is reflected over all angles, it does not provide the information required to model stray light reaching the focal plane of an optical system. This is because much of the light is blocked or scattered back by instrument components such as mirrors, baffles, or stops. NASA utilizes ray-tracing codes that deterministically calculate the trajectory of all light that propagates through an optical system. For mirrors and optical elements measurements of the surface figure and micro-roughness and allocations for contamination are required to create this model. For structural elements and stray light controls such as baffles, tubes and stops the distribution of light scattered over specific angles is required. The bidirectional reflectance distribution function (BRDF) defines the directional reflection characteristics of an optical surface. It provides the reflectance of a target in a specific direction as a function of illumination and viewing geometry. The BRDF is a function of wavelength and reflects the structural and optical properties of the surface. The BRDF definition and derivation are credited to Nicodemus et al. [4] who examined the problem of defining and measuring the scatter of diffuse and specular optical materials. Following his concept the scatter defining geometry is shown in Figure 4, where the subscripts i and s refer to incident and scatter quantities, respectively. He also assumed that all scatter comes from the sample surface and none from the bulk. He defined the BRDF in radiometric terms as the ratio of the surface radiance L_s scattered by a surface into the direction (θ_s, ϕ_s) to the incident surface irradiance E_i incident on a unit area of the surface at a particular wavelength:

$$BRDF = \frac{dL_s(\theta_i, \phi_i, \theta_s, \phi_s; E_i)}{dE_i(\theta_i, \phi_i)} \quad (1)$$

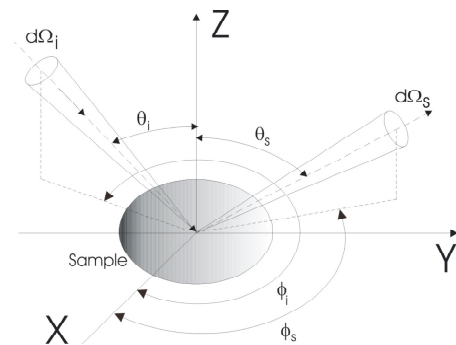


Figure 4. Scattering geometry

where the subscripts i and s denote incident and scattered respectively, θ the zenith, and ϕ the azimuth angles.

The various carbon nanotube samples were measured in the Diffuser Calibration Facility at NASA's Goddard Space Flight Center (GSFC) using the facility's scatterometer. The scatterometer, located in a class 10000 laminar flow cleanroom, is capable of measuring the BRDF of a wide range of sample types including white diffusers, gray-scale diffusers, black painted or anodized diffusers, polished or roughened metal surfaces, clean or contaminated mirrors, transmissive diffusers, liquids, and granular solids. The operational spectral range of the instrument is from 230 nm to 900 nm. The scatterometer facilitates computerized measurements at selected incident and scattered geometries and wavelengths for complete data acquisition. The measurement uncertainty, ΔBRDF , depends on several instrument variables. It was evaluated in accordance with NIST guidelines [5] to be less than 1% standard uncertainty. The main sources of uncertainty are 1) signal to noise ratio; 2) nonlinearity of the detector and electronics; 3) receiver solid angle; and 4) the total scatter angle error. The main sources of error are considered independent. Schiff et al. [6] presents the detailed study on measurement uncertainty. Figure 5 shows the goniometer mechanism of the scatterometer. The scattered light from the sample is collected using an ultraviolet-enhanced silicon photodiode detector with output fed to a computer-controlled lock-in amplifier. The sample is mounted on a stage in the horizontal plane. The sample stage allows proper positioning of the sample with respect to the incident beam. It can be moved in X, Y and Z linear directions using three motors. The sample stage provides sample rotation in the horizontal plane around the Z axis enabling changes in the incident azimuth angle, ϕ_i . Sample stage leveling is adjustable using two manual micrometers. Various holders are available to support samples of different sizes, shapes, and thicknesses.

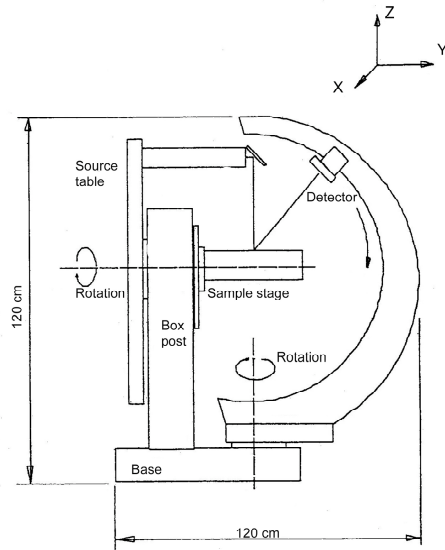


Figure 5. Scatterometer goniometer

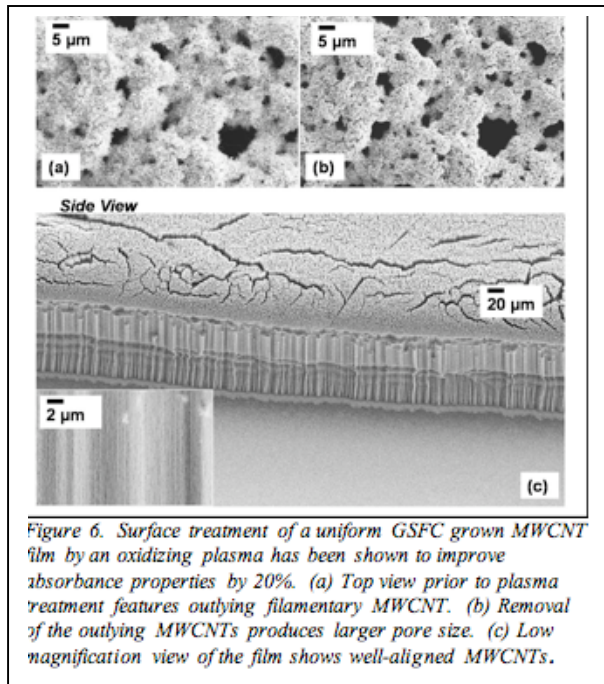
3. METHODOLOGY FOR NANOTUBE GROWTH AND OPTIMIZATION

Development of this technology for use in space flight instrumentation required three stages of development. Stage 1 required tuning the nanotube geometry to produce the desired low reflectance over all angles on silicon. The second stage required improved adherence of the film onto silicon. The third stage was a demonstration of the deposition of nanotubes onto alternate materials more suitable for components that would be placed under higher mechanical stresses due to their placement in the instruments.

3.1 Growth on Silicon Substrates

Hemispherical reflectance measurements on initial samples grown at GSFC showed about 5% total integrated scatter, approximately on par with standard surface treatments such as Z306 paint. Our goal was to achieve an order of magnitude improvement. Several promising avenues for optimization of MWCNT geometry were attempted to minimize the total integrated scatter. Areas that were investigated include:

1. Use O_2 plasma etch to add roughness and porosity to the MWCNT film.
2. Use surface roughness to engineer the morphology of catalyst-assisted thermal chemical vapor deposition grown MWCNT film.
3. Dependence of CNT reflectance as a function of catalyst thickness; thin catalyst was expected to correlate with low-density, tall MWCNT films [7]



Fabrication of vertically oriented MWCNT films was accomplished by catalyst-assisted chemical vapor deposition (CVD). Using silicon as the growth substrate, the fabrication begins with the thermal deposition of aluminum/iron thin film catalyst. To grow MWCNTs, the substrate is exposed to ethylene feedstock gas at 750°C in a reducing environment; the ethylene is dissociated at the iron surface, and the carbon is extruded in the form of a dense film of aligned MWCNTs. Precise patterning of the MWCNT film can be accomplished by constraining the placement of the catalyst film through conventional lithographic means. Varying the catalyst thickness on the substrate can modulate the MWCNT height.

Following approach 1 above, an increase of measured absorbance of about 20% was achieved by treating the MWCNT film with plasma oxidation, which increases porosity at the MWCNT film surface. Figure 6. is a scanning electron microscope (SEM) image of the sample before and after plasma “cleaning”.

Following approach 2, we roughened the substrate by mechanical means or basic grinding with various grit sizes. Again this resulted in only small improvements in the amount of light that was reflected. Work continues in this area to

determine if further improvements can be made.

Following approach 3, we simply used the modulation of catalyst film thickness to produce low-density, tall MWCNTs. We studied the extreme regime of catalyst thickness to characterize the limits of this technique to producing low MWCNT fill factors. At very low catalyst thickness, however, we anticipate that we will be limited by the uncertainty in controlling the thickness of the film using standard vacuum deposition techniques. Minimization of catalyst film thickness resulted in an order of magnitude improvement in the performance of the MWCNT as an absorber. Our process resulted in multiwalled carbon nanotubes with inner diameters of 1-5 nm, outer diameters of 30-100 nm and average spacing of 100-500 nm. The best samples had lengths of 50 to 100 microns, but it is highly probable that longer lengths would provide better performance and we are actively pursuing this area since researchers at Rensselaer Polytechnic Institute have reported achieving even higher absorption with longer nanotubes[8].

3.1 Adhesion enhancement on silicon

Carbon nanotubes grown on silicon with only the iron catalyst layer exhibit poor adhesion; it is quite easy to rub the nanotubes off of the substrate with any contact. Utilization of MWCNTs in space flight hardware requires that they are robust to prevent degradation of the coating or contamination of critical components. Previous work suggests that the point of failure is at the catalyst-substrate interface. We explored alternative substrate preparation techniques to improve adhesion. The primary approach we developed was the use of a thin-film sticking layer under the iron catalyst layer. We experimented with chromium, titanium and alumina underlayers. The approach was straightforward and should not have significantly impacted the favorable properties of the thin Fe catalyst film. What we found however was that the nanotube growth properties were significantly affected by this layer. After much trial and error, it was determined that alumina provided a good sticking layer without degrading the optical properties of the carbon nanotubes. Figure 7 is a SEM image of a section of the nanotube layer that was physically removed to allow inspection. In general the film is uniform, oriented and quite robust to physical contact.

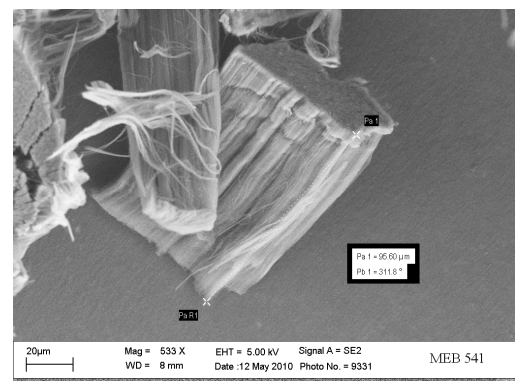


Figure 7. MWCNTs on silicon with alumina underlayer for enhanced adhesion

3.2 Growth on alternate materials

It is quite feasible to use silicon for a variety of elements in space flight instrumentation including mirrors, slits and small blocking elements such as coronagraphic masks. However, silicon is quite brittle and is not the material of choice for elements that may be subjected to structural loads such as baffles and stops. To address the need for nanotube growth on materials that were more suitable for these elements we either grew nanotubes on alternate materials at GSFC or acquired them from our collaborators. Hemispherical reflectance measurements are shown for each CNT sample in Figure 11.

The substrates investigated at GSFC included stainless steel, nickel and titanium using the same thickness of iron catalyst layer and growth parameters optimized on the silicon substrates. Figure 8 is a SEM image of growth on titanium. While the titanium was second best to silicon in terms of performance, the growth appeared quite different with features that looked more like wires and seemingly random arrangements of curled nanotubes. Stainless steel and nickel substrates did not result in acceptable nanotube growth.

CNTs were also grown at the Applied Physics Laboratory (APL; Papadakis et al.) on titanium and alumina substrates for evaluation. Low cost alumina substrates resulted in very poor growth or samples that were black but quite shiny. The best results were on commercially available Synkera (Syntek) alumina substrates, these were however only marginally better than the Z306 paint. The alumina substrate samples also have a more crystalline appearance see Figure 9, with no clear alignment of what appear to be very fine nanotubes. Titanium samples grown at APL were not quite as dark as those grown at GSFC.

In addition, samples grown on Inconel and on silicon with sub-millimeter and millimeter tube height were grown at the University of Southern Illinois (Dr. Saikat Talapatra). The inconel substrate samples reflectance were about 40% better than paint over the optical band that they were measured. Again SEM images, Figure 10, show that the nanotubes are not aligned and in fact randomly oriented or clumped together into “ropes” of nanotubes.

The growth of the long aligned MWNTs on Silicon oxide substrates was achieved by using a air assisted chemical vapor deposition technique in which a horizontal tube furnace was heated to 790°C in an argon environment, and a solution of ferrocene and xylene (about 1 gm in 100 ml of Xylene) was continuously injected, vaporized, and blown (using argon and hydrogen (85%/15%) as carrier gas) into a quartz tube reactor containing the inconel substrates. The flow rate of carrier gas was maintained at about 500 sccm. During the growth process, a small amount of air (~ 5 sccm) was mixed with the reaction environment to maintain the catalyst activity facilitating enhanced growth rate. The quartz tube reactor was cooled down to room temperature after growth time in the argon environment. We obtained an array of densely packed aligned multiwalled carbon nanotubes on the Silicon Oxide substrates, which was removed (using a razor blade) for measuring the optical properties.

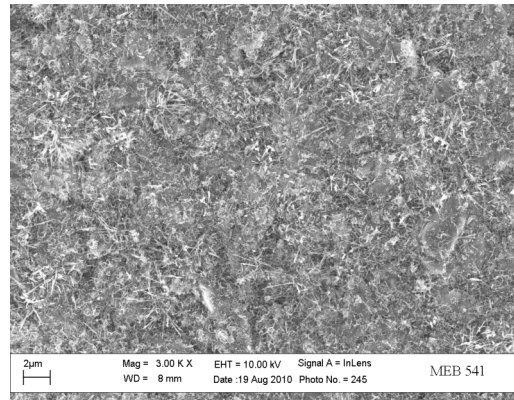


Figure 8. Growth on Titanium

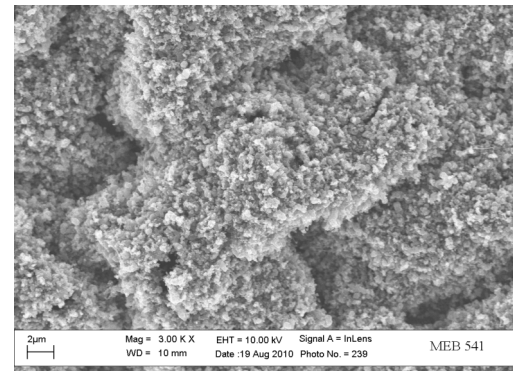


Figure 9. Growth on Alumina

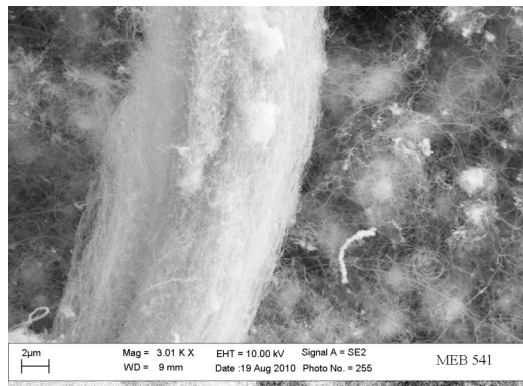


Figure 10. Growth on Inconel

Figure 8 shows the measured hemispherical reflectance of Z306 paint (the standard blackening surface treatment for spacecraft parts), and carbon nanotubes grown on inconel, titanium and silicon with and without the alumina layer used for enhanced adhesion. The best samples approach the desired factor of 10 improvement over the Z306 paint in terms of total integrated scatter.

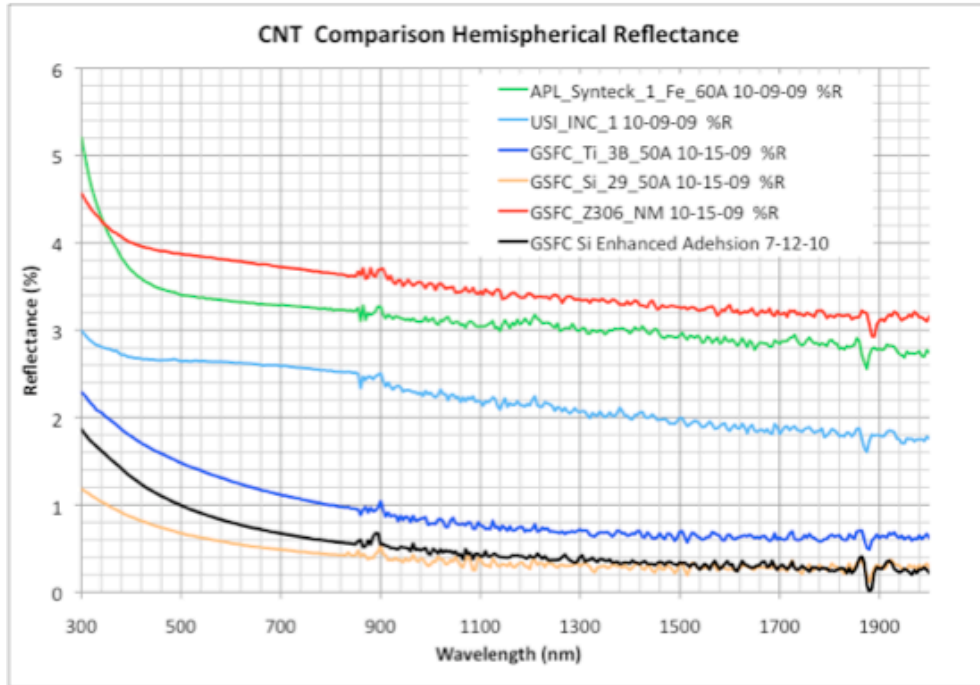


Figure 11. Carbon nanotube hemispherical reflectance for a variety of substrates

BRDF measurements were also performed on the samples to assess the directional dependence of light that is scattered by various samples to allow system modeling. Figures 12a,b are NIST traceable measurements of the MWCNT samples. It is interesting to note that at 900 nm wavelength there appears to be a larger near on-axis specular component that may be attributable to long wavelength radiation penetrating deeper into the nanotube layer and reflecting off of the shiny silicon substrate on the GSFC silicon samples. This is not observed in the SIU millimeter length nanotube samples, even though the average reflectance over all angles is higher. This may be because the SIU samples are higher

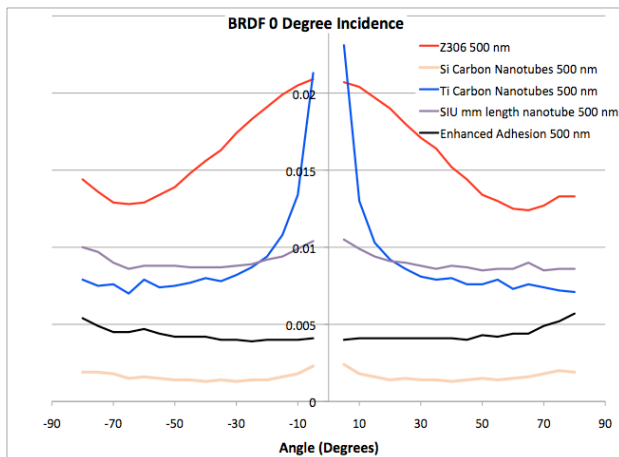


Figure 12a. BRDF at 500 nm wavelength

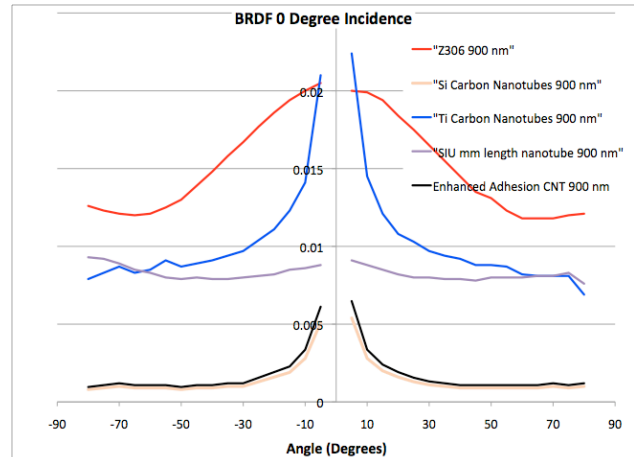


Figure 12b. BRDF Measured at 900 nm wavelength

density and therefore present a higher index change to the incident light. Future efforts will seek to maintain low-density nanotubes while creating a thicker mat to maximize absorption.

4. EXAMPLE OF ASTROPHYSICS APPLICATIONS - LISA

The Laser Interferometer Space Array (LISA) experiment, included as a prioritized mission in the 2010 NRC Astronomy and Astrophysics Decadal Report [9] seeks to detect gravitational waves from cosmological sources. LISA utilizes a constellation of three science craft spaced at 5 million kilometers. The sciencecraft are all linked to each other using telescopes that are used in duplex to transmit and receive phase locked laser reference beams. Figure 13 is a representation of the sciencecraft triad with a block diagram of the optical system in Figure 14. A proof mass is located in each science craft and the interferometers continually monitor the path lengths between sciencecraft to detect length changes due to gravitational waves stretching space. The power in the transmitted beam is 9 orders of magnitude higher than that of the received beam in each telescope. The engineering challenge is to detect the received beam phase with a high enough signal to noise to allow measurement to femtometer accuracies. Since exquisite wavefront error stability is required in the telescopes, it is probable that they need to be used on axis, which leads to the need for extraordinary stray light control.

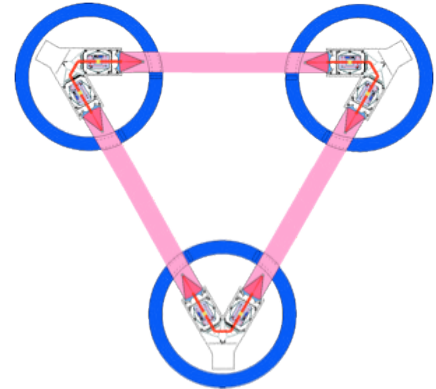


Figure 13. LISA Sciencecraft triad

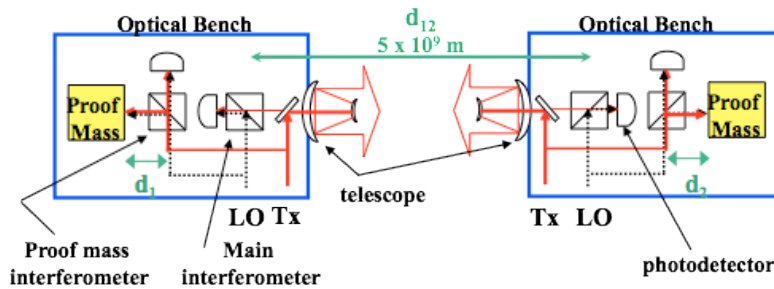


Figure 14. LISA block diagram

4.1 Optical Model of the LISA Telescope

The transmitted laser beam is expanded to fill the telescope secondary mirror and then is reflected to the primary mirror to send a collimated beam between the sciencecraft. A representation of the optical layout of the LISA system is shown in Figure 15. The expanding transmitted beam fills the entire secondary mirror, simultaneous with the received beam, which is directed off of the primary mirror. The received beam is however, obscured in the center of the secondary mirror by its own shadow. The issue is that the transmitted signal is nearly on axis to the center of the secondary mirror and will scatter light back to the focal surface and photodetector. In this case the transmitted beam is 9 orders of magnitude higher in intensity and must be suppressed. This can be accomplished by blackening the center of the secondary mirror or by putting a hole in the center of the secondary mirror with an absorber in the back of it. We believe that the best solution is to use carbon nanotubes for this purpose and that silicon is a good candidate substrate. High quality (better than $1/200$ waves surface figure); single crystal silicon mirrors have been fabricated by NASA GSFC. [10]. The additional benefit of this extraordinarily stable substrate is that it amenable to direct growth of

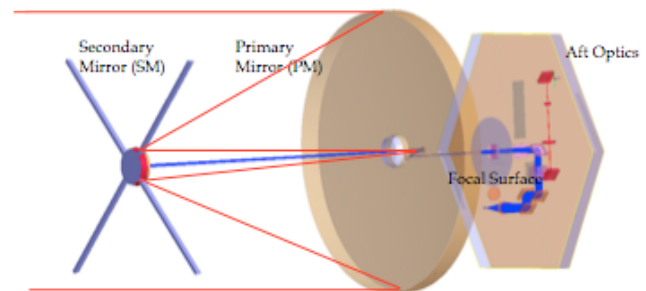


Figure 15. LISA Telescope is used in Duplex

carbon nanotubes without compromising its figure during growth in the 750 C furnace. Therefore, it was decided to evaluate the performance of a MWCNT mask as the center of the secondary, a Z306 mask and a circular hole.

4.2 Modeling stray light in FRED

FRED is a ray trace code used at the Goddard Space Flight Center to model end to end optical systems and evaluate image quality, ghosting and stray light. It requires high fidelity data on each element of the optical system including figure, micro roughness, contamination levels and BRDF for any structural materials in the optical path or adjacent to it. FRED tracks multiple bounces due to scattered light (such as that from a bare mirror, a nanotube or paint patch or the edges of a hole) and propagates them through the system. In this case, there is a direct path to the focal plane, a path that requires scattering to the primary mirror and direct reflection off the secondary mirror back to the focal plane etc. that is tracked. June Tveekrem of the GSFC Optics Branch, modeled the LISA system using FRED. The results of the trade are shown pictorially in Figure 16.

The carbon nanotube patch is a factor of 11 better than the Z306 paint, but a factor of 2 worse than the hole in the secondary mirror for when the total irradiance reaching the detector is calculated. This however does not take into account the implementation of beam dump behind the hole (since an open hole would provide a direct stray light path

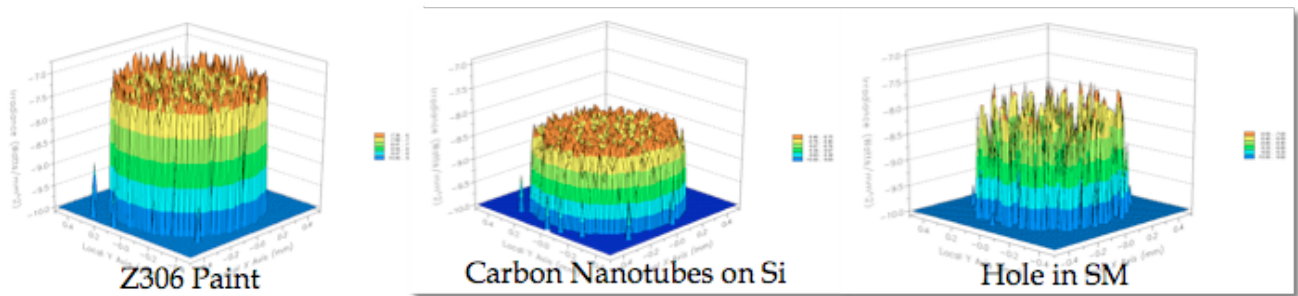


Figure 16. FRED Analysis of scattered light reaching LISA focal plane from secondary mirror

from bright stars) or the difficulty in fabricating a hole in the mirror. In addition, when peak irradiance is evaluated the nanotubes provide a more uniform background than the hole.

4.3 Additional means of controlling stray light using nanotubes

In conjunction with other work we have found that nanotubes can be grown to desired patterns by using lithographic masks to control the areas of catalyst deposition. This makes it possible to further reduce the stray light in the LISA telescope by moving from a circular shaped mask to a shape that minimizes diffraction. This approach is called apodization and is used in stellar occulting designs that NASA is developing to block out bright stars to allow viewing of dim companions. Ron Shiri of the GSFC Optics Branch, utilized diffraction codes used for these occulter systems to find an optimal shape for the carbon nanotube patch on the secondary mirror by iterating on several petaled shapes. He evaluated several shapes and compared the near field diffraction to that observed using a circular shape shown in Figure 17. In this case a 6 petal hyper gaussian shape provided an astonishing 8 orders of magnitude suppression in the zone of interest. Only a small portion of this diffracted light makes it to focal plane due the instrument geometry. Therefore it was required that the shape be modeled in FRED to determine the actual benefit of the apodization mask to reduced stray light. Figure 18. shows the impact of this apodization on the contribution of stray light. The petaled mask reduces the amount of stray light due to the central patch by a factor of 2 over the simple

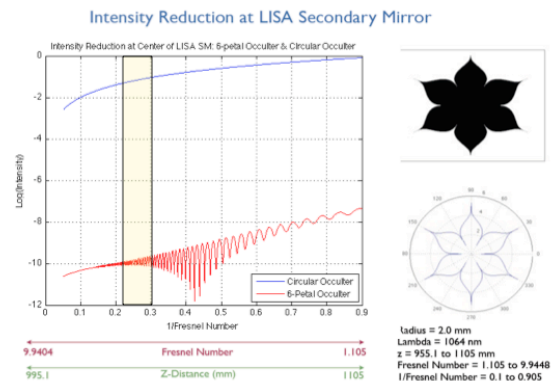


Figure 17. Hypergaussian shaped mask reduces diffraction from nanotube patch on secondary mirror

circular mask. Due to the high incident power, even the carbon nanotube central patch resulted in the secondary being the highest source of stray light. With the hypergaussian shaped mask the contribution to stray light from the secondary

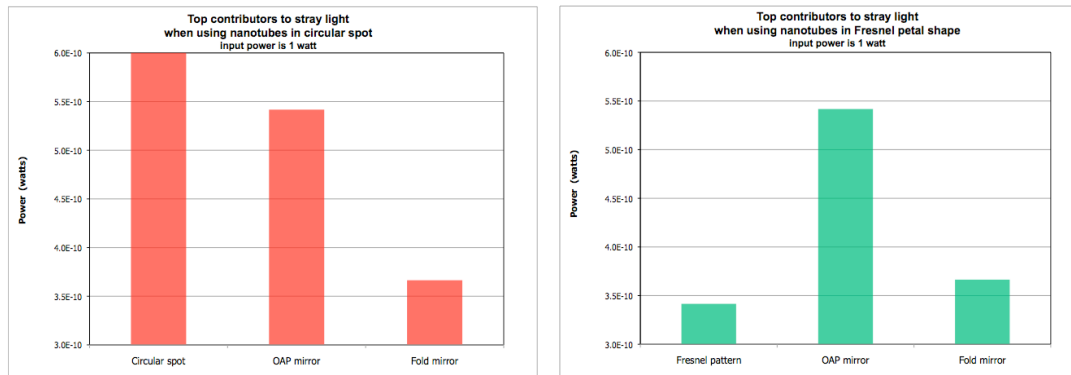


Figure 19. Comparison of top 3 sources of stray light in LISA before and after shaping of nanotube patch to hypergaussian petal shape.

mirror is reduced by a factor of 2 making it the smallest of the top 3 contributors to stray light. It is possible that even greater stray light reduction can be obtained when the shape is optimized for far field diffraction suppression.

REFERENCES

- [1] Space Studies Board, Division on Engineering and Physical Sciences, National Research Council of the National Academies, "Earth Science Applications from Space: National Imperatives for the Next Decade and Beyond", The National Academies Press, Washington, DC, (2007).
- [2] Butler, J.J. and R.A. Barnes, 'Calibration Strategy for the Earth Observing System (EOS)-AM1 Platform, IEEE Transactions on Geoscience and Remote Sensing, 36, 1056-1061 (1998). Van Derlofske, J. F., "Computer modeling of LED light pipe systems for uniform display illumination," Proc. SPIE 4445, 119-129 (2001).
- [3] Qiu, S., G. Godden, X. Wang, and B. Guenther, "Satellite-Earth Remote Sensor Scatter Effects on Earth Scene Radiometric Accuracy," Metrologia, 37, 411-414 (2000).
- [4] F.E. Niodemus, J.C. Richmond, J.J. Hsia, I.W. Ginsburg, and T. Limperis, "Geometrical considerations and nomenclature for reflectance", National Bureau of Standards, NBS monograph 160, (Oct. 1977).
- [5] B.N. Taylor and C.E. Juyatt, "Guidelines for Evaluating and Expressing the Uncertainty of NIST Measurement Results", NIST Technical Note 1297, US Dpeartment of Commerce, National Institute of Standards and Technology, (Sept 1977).
- [6] T.F. Schiff, M.W. Kighton, D. J. Wilson, F.M. Cady, J.C. Stover, and J.J. Butler, "A Design Review of a High Accuracy UV to Near Infrared Scatterometer", Proc. SPIE, 1995, 121-130 (1993)
- [7] Getty, Stephanie A.; Bis, Rachael A.; Snyder, Stacy; Gehrels, Emily; Ramirez, Kristina; King, Todd T.; Roman, Patrick A.; Mahaffy, Paul R, "Effect of nitrogen gas on the lifetime of carbon nanotube field emitters for electron-impact ionization mass spectrometry," Proceedings of the SPIE 6959, 695907 (2008).]
- [8] Zu-Po Yang, Lijie Ci, James A. Bur, Shawn-Yu Lin, and Pulickel M. Ajayan, "Experimental Observation of an Extremely Dark Material Made by Low-Density Nanotube Array," Nano Letters 8, 446 (2008)
- [9] Committee for a Decadal Survey of Astronomy and Astrophysics; National Research Council, "New Worlds, New Horizons in Astronomy and Astrophysics," National Academies Press (Washington, DC),(2010.)
- [10] Vincent T. Bly, David A. Content, John G. Hagopian, and Linette D. Kolos, "Light weight mirrors from single crystal silicon" Proceedings of SPIE, Vol. 5179, 262 (2003)